**Proceedings of ICFDP9:**
**Ninth International Congress of Fluid Dynamics & Propulsion**
**December 18-21, 2008, Alexandria, Egypt**

**ICFDP9-EG-213**

# COMPARISON OF PERFORMANCE OF A WIND-DRIVEN VENTILATOR UNDER LABORATORY AND FIELD CONDITIONS

**M.A.Serag-Eldin**
**Mechanical Engineering Dept,**
**American University in Cairo, Egypt.**
**e-mail:AmrSerag@AUCEgypt.edu**

## ABSTRACT

The paper presents the results of comparison of the performance characteristics of a model of a wind-driven venturi-type room ventilator, under both laboratory and field conditions. It is revealed that although minor differences exist between field and laboratory conditions, the effect on performance is remarkable. The paper analyzes the cause of this discrepancy using state of the art software. It serves to warn against similar cases, where by necessity small deviations exist between experimental and field operational conditions, and it is commonly assumed that they have no bearing on the results, yet they do.

## KEYWORDS:

Venturi-flow, turbulent flow, experimental validation, modeling and simulation, performance prediction.

## INTRODUCTION

In a previous study, a new design for a wind driven venturi-type ventilator was presented [1]. Since the design was developed entirely employing computational modeling, experimental validation was sought at a later date. Thus a physical model was built true to shape and its performance was tested experimentally, [2]. Although the experimental conditions were initially assumed to be sufficiently close to the field conditions that the measured performance would be same as that predicted under simulated field conditions, it was found that there was considerable deviation between the two. At first the accuracy of the computational model(particularly the turbulence model) was questioned; however when the boundary conditions of the mathematical model were modified to represent closely the experimental conditions rather than field conditions, very good agreement was observed, thus validating the mathematical model. It thus become clear that the difference in performance is due to the small deviations in boundary conditions.

In the present paper, the causes of the discrepancies are further investigated. First the considered wind-driven ventilator is introduced. The experimental rig is then described. The employed governing equations are introduced together with the adopted boundary-conditions, and both the predicted field performance and predicted laboratory performance are compared. An investigation is then conducted to reveal why large differences in performance exist despite what apparently looked like similar operating conditions.

## THE VENTURI VENTILATOR

As the name implies, the ventilator design investigated here exploits the venturi principle. Figure 1 displays a sketch of an isometric cut through the mid-plane of the device.

Atmospheric wind is guided into a converging channel to increase its speed and decrease its pressure. The minimum pressure occurs near the throat section; the partial vacuum is then employed to suck in air from the enclosure to be ventilated.

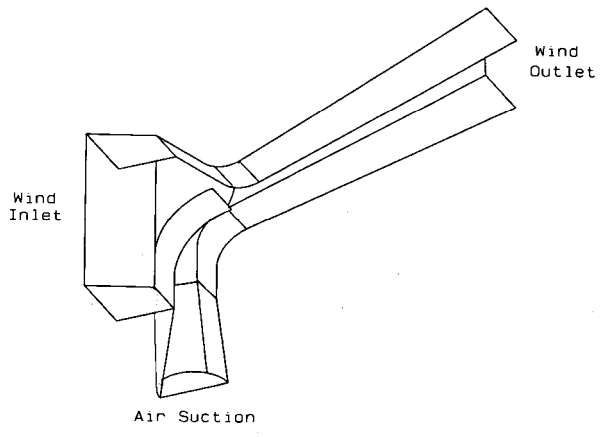


Figure 1. Isometric sketch of mid-plane cut of wind-ventilator.

## THE EXPERIMENTAL RIG

A sketch of the experimental rig, with the tunnel and model contours drawn to scale, is shown in Fig. 2.; dimensions are in cms. The rig features an induced draft wind tunnel with an extended inlet section. The wind tunnel inlet displays a smooth bell-mouth followed by a uniform square section of 0.77 m sides and 0.90 m length. The ventilator model is fixed to the floor of the inlet section with its suction pipe extending downwards and protruding out of the wind tunnel bottom.

The model suction pipe is approximately 51 m.m. in diameter. It features a bell mouthed inlet followed by a 45 cms straight length of pipe, followed by a venturi-meter with a 32 m.m. throat diameter. The venturi-meter is connected directly to the ventilator inlet section. It is employed to measure the inlet suction flow rate, with the aid of an inclined manometer. At its widest point (inlet to the guide vanes) the model width is 11 cm and its maximum height above the floor of the inlet section is 41 cm. The frontal area of the model including the suction pipe is approximately 4 % of the inlet section area.

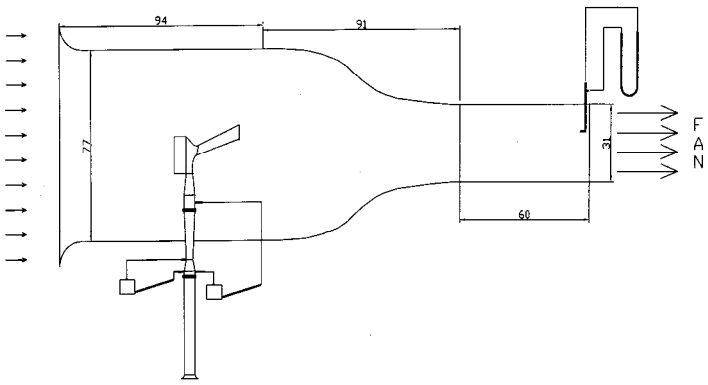


Figure 2. Sketch of experimental apparatus.

A pitot-static tube connected to a vertical U-tube water manometer is employed to measure the flow velocity at the end of the long straight section of the tunnel following the convergent nozzle; this is the exit section displayed in Fig. 2. Originally the straight section was the designed working section of the tunnel; however it was decided to place the model at inlet section after modifying and extending it so as to host a larger model size. The straight section is square with 30.5 cm sides, and is 61 cms long. Beyond the exit section is the wind tunnel fan section (not displayed).

## MATHEMATICAL MODEL

The computational model employed to predict the flow field under various boundary conditions is described here.

### *A. Governing Equations and Grid System*

The computational model comprises fully three-dimensional elliptic differential equations expressing conservation of mass, balance of momentum in three directions and transport of the kinetic energy of turbulence, k, and it's rate of dissipation, ε; the later two equations being introduced by the adopted Renormaliation Group(RNG) k-ε turbulence model [3],[4]. The equations are discretized employing a finite volume method ,e.g.[5] and solved by a variant of the SIMPLE algorithm [6].

In order to express the wall boundary conditions accurately, a three-dimensional, non-orthogonal boundary fitted coordinate system is employed [7]. Elliptic grid generation [8] is adopted to generate the Cartesian coordinates of the control volume corner points. Fig. 3 displays a part of the BFC grid in the vertical plane passing through the mid-section of the ventilator.

It is noticed that the grid-lines are too densely packed in some regions to be discernable. The compacting of grid lines is due to the need for high resolution in certain regions, as well as the outcome of the grid curvature required to give a high level of grid orthogonality. Due to symmetry the integration domain covers only one half of the wind-tunnel cross-section.

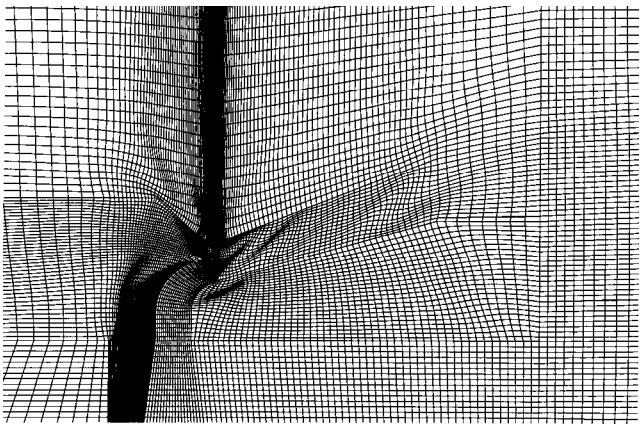

Figure 3. Boundary-fitted-coordinates around ventilator body.

Details of expressing the convection and diffusion terms in boundary fitted coordinates may be found in [9],[10]; essentially, the control volume equations state:

$$C_\phi = D_\phi + S_\phi \qquad (1)$$

where $C_\phi$ expresses the net rate of convection of the variable $\phi$ out of the control volume, $D_\phi$ expresses the net rate of diffusion of $\phi$ into the control volume, and $S_\phi$ expresses the sum of sources of $\phi$ within the control volume. The mass conservation equation may also be expressed in the form of (1) with neither diffusion nor source terms. For the momentum equations the source terms represent the pressure gradient terms, whereas for the k -equation the source terms represent the difference between the generation and dissipation rates. For the ε-equation the source term is $S_\varepsilon = [C_1 G_k - C_2 \rho\varepsilon] \varepsilon/k. + R$, where $G_k$ denotes the generation rate of k, $C_1$ and $C_2$ are turbulence model constants whose values are displayed with the other model constants in Table I, and R denotes the source

term from renormalization. The latter is expressed by the following relation:

$$R = \rho \frac{C_\mu \eta^3 (1 - \eta/\eta_o)}{1 + \beta \eta^3} \frac{\varepsilon^2}{k} \quad (2)$$

where:

$$\eta = S\frac{k}{\varepsilon}, \quad S = (2S_{ij}S_{ij})^{1/2}, \quad S_{ij} = \frac{1}{2}\left(\frac{\partial u_i}{\partial x_j} + \frac{\partial u_j}{\partial x_i}\right) \quad (3)$$

The momentum diffusion terms employ a velocity gradient expression with an eddy diffusivity, $\mu_t$ derived from k and ε according to:

$$\mu_t \equiv \rho\, C_\mu\, k^2/\varepsilon \quad (4)$$

where $C_\mu$ is another turbulence model constant. The eddy diffusivity terms for k and ε are expressed by $\mu_t/\sigma_k$ and $\mu_t/\sigma_\varepsilon$, respectively , $\sigma_k$ and $\sigma_\varepsilon$ being turbulence model constants.

Table I. Turbulence model constants

| $C_1$ | $C_2$ | $C_\mu$ | $\sigma_k$ | $\sigma_\varepsilon$ | β | $\eta_o$ |
|---|---|---|---|---|---|---|
| 1.42 | 1.68 | .0845 | 0.7194 | 0.7194 | 0.012 | 4.38 |

### *B. Boundary Conditions*

First the boundary conditions employed to represent "field conditions" are presented; then the boundary conditions representing more closely the "experimental conditions" are displayed.

B.1 Field Boundary Conditions

The integration domain in this case is box shaped and displays the following boundaries:

i) the bottom boundary

it comprises the roof of the enclosure to be ventilated; it is assumed to be a horizontal, impermeable, wall-boundary except for the opening of the suction channel. Wall boundary conditions, i.e. no slip and wall functions [11], are therefore applied at the roof; with the exception of the channel cross-section itself, where a constant total-pressure, $P_o$, condition is imposed. Furthermore, the flow is assumed to enter the suction channel with only an axial component of velocity.

ii) the top boundary:

this is a no-flow, slip-boundary. It is parallel to the bottom boundary and raised sufficiently high above the ventilator top that it does not affect the suction flow rate. Vertical gradients of dependent variables are assumed to be zero at this boundary.

iii) the upstream boundary

this is located far enough upstream the ventilator that the flow there may be assumed to be unperturbed by its presence and conditions may be taken to be those corresponding to free atmospheric wind flow. A uniform static-pressure, $p_{st}$ , equal to the prevailing atmospheric pressure is specified at this boundary. The inlet turbulence energy is assumed to be 1% of the inlet mean flow kinetic energy. The inlet value of ε is calculated from the inlet value of turbulence and a length scale equal to 0.4* mean height of inlet section from roof-top.

iv) the far downstream boundary

this lies at opposite ends to the upstream boundary, and is located far enough downstream the diffuser exit section that downstream effects are not transmitted upstream. Moreover it is assumed that the flow leaves this section longitudinally with the specified uniform free-wind speed

v) the symmetry plane

this is the vertical mid-plane of the ventilator. Symmetry boundary conditions are imposed there; they imply no-flow and absence of normal gradients.

vi) side boundary:

this is the far-side, lateral vertical-plane lying at opposite end to the symmetry-plane and at a sufficient distance from it that the flow there may be assumed to correspond to the undisturbed free-wind. Similar to the top boundary, this boundary is also a no-flow, slip-boundary, with absent normal gradients of dependent variables.

In addition to the above, wall boundary-conditions , [11], are imposed at all the internal and external surfaces of the ventilator walls and partitions.

B.2 Experiment Boundary Conditions

Here, the integration domain follows the contours of the wind-tunnel from inlet to the end of the test section, terminating immediately upstream the fan duct. The boundary conditions are specified to represent the experimental conditions as faithfully as possible. The following type of boundaries and conditions are encountered:

i) inlet boundary

this corresponds to the wind tunnel inlet section, right after the bell mouth. A total pressure boundary condition is imposed there; with the total pressure equal to atmospheric pressure and the inlet axial velocity component solved for. The fluid is assumed to enter with negligible cross-stream and vertical velocity components, and with a uniform value of k equal to 1% of the inlet mean flow kinetic energy. The inlet value of ε is calculated from the inlet value of turbulence and a length scale equal to 0.4* average distance from wall boundaries( quarter height of inlet section).

ii) wall boundaries

these comprise the inner walls of the wind tunnel, and both the inner and outer walls of the model. No slip, smooth wall, equilibrium wall functions are applied at those boundaries [11]. They imply the calculation of the wall shear stress from a logarithmic function.

iii) exit section

this corresponds to the downstream-end of the original wind-tunnel test-section, the section immediately upstream the fan section. A uniform value of $W_{ex}$ is specified at this boundary, while the pressure is solved for. The value of $W_{ex}$ is specified to be the experimentally measured one. The flow is assumed to leave this boundary with the same properties as for the immediate upstream calculation plane.

iv) suction-pipe boundary

this corresponds to the suction pipe cross-section at the floor of the wind tunnel. The actual suction pipe used in the experiment extends further down than that, protruding a considerable distance below the wind tunnel floor, Fig. 2. Moreover it includes a bell mouthed inlet, straight length of piping, a venturi-meter, and an upstream and downstream sleeve to attach the venturi- meter to the pipe and model inlet, respectively.

However for the purpose of the present analysis the extra complication involved in protruding the integration domain and modeling the flow within the venturi-meter is considered unnecessary. Instead the flow losses between the inlet of the suction pipe and the inlet of the model are estimated from common practice, whereas the total loss in the venturi-meter is actually based on experimental measurements at the highest wind speed. It equals approximately 11% of the measured pressure difference between venturi-throat and inlet. This compares well with the 10-15 % reported in the literature [12].

A total pressure boundary condition is specified at this boundary with the total pressure equal to atmospheric pressure. The pressure drop due to the miscellaneous losses in the suction pipe is spread uniformly over the entire length of the pipe. The inlet suction velocity $V_{suc}$ is solved for at the boundary, and the other velocity components are neglected. The inlet value of k is specified to be 1% of $V_{suc}^2$, and ε is calculated from that value of k and a length scale equal to 0.4 x average radius of pipe. According to estimates, the total suction pipe loss is equal to $V_{suc}^2/2g$; however a value of 0.85 $V_{suc}^2/2g$ is used instead as it gives excellent agreement with measurements.

v) symmetry plane

this is the vertical mid-plane of the ventilator. Symmetry boundary conditions are imposed at this boundary.

## MODEL VALIDATION

Model validation was reported elsewhere [2], but is repeated here for sake of completeness. Figure 4, reproduced from [2], compares the results of computations made employing experimental boundary conditions versus corresponding measurements. The diagram presents suction velocity versus wind-tunnel entry velocity; the former represents the output of the device whereas the latter represents the input; hence Fig 4 represents the performance characteristics of the device.

Two lines of predictions are displayed, corresponding to inlet pipe losses of $V_{suc}^2/2g$ and 0.85 $V_{suc}^2/2g$. For the latter case in particular, the agreement between measurements and predictions is seen to be excellent, thus validating the model.

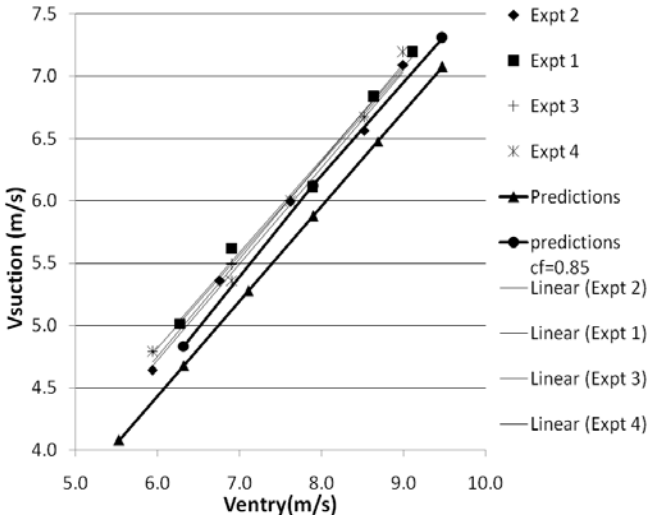


Figure 4. Comparison between measurements and predictions

## MEASURED & PREDICTED PERFORMANCE

Having established confidence in the predictions of the computational model, comparison is now made between predicted results corresponding to the simulated field conditions, and those corresponding to the laboratory conditions with both original and modified boundary conditions, Fig. 5.

The blue trend-line displaying circular-markers reveals the predicted performance curves for field conditions, while the red one displaying square-markers displays the predicted performance curves under pure laboratory conditions, i.e. a total pressure condition of $P_o$=0 at entrance to wind tunnel, and a head loss at suction inlet, $h_L = 0.85V_{suc}^2/2g$ .

Although both characteristics reveal the same linear trend, the laboratory-conditions curve displays considerably larger suction velocities for same entrance wind speed, indicating that the measurements over-predict the true performance of the device under field conditions.

In order to investigate the cause of this discrepancy, the laboratory boundary conditions are modified one at a time to approach the field boundary conditions. Thus, for the same experimental integration domain, predictions are also made for each of the following two conditions:

i) Specified inlet static pressure $p_{st}$=0 rather than $P_o$=0; all other conditions corresponding to laboratory conditions. The results are displayed in the form of the green trend-line displaying triangular-markers.

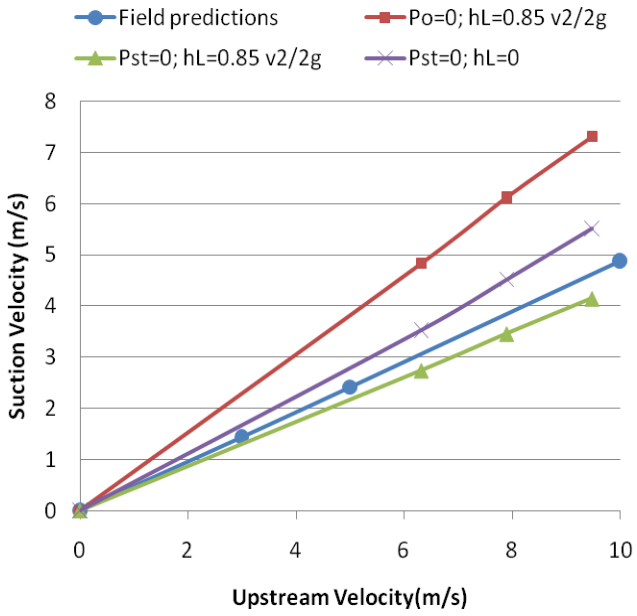


Figure 5. Comparison between field and lab performance

ii) Specified inlet static pressure $p_{st}$=0 as well as $h_L$=0 instead of $h_L = 0.85v_{suc}^2/2g$; all other conditions corresponding to laboratory conditions. The results are displayed in the form of the purple trend-line displaying cross-markers.

Comparison between the latter two cases and field conditions, reveals that the replacement of the total pressure-condition with the static-pressure conditions resulted in marked improvement of results. Thus it is concluded that this deviation in laboratory condition from field condition is the primary factor responsible for the difference in predicted performance.

Figure 5 also shows that retaining suction-inlet losses at their laboratory value reduces performance beyond that of the field, which is to be expected. However, when both $p_{st}$=0 and $h_L$=0, it is expected to get the same results as the field performance, which is not the case. Indeed the results in that case deviate even further from the field conditions than in the former case; albeit over-predicting rather than under-predicting.

The explanation must lie in that there is another source of deviation in performance between field and laboratory, and that it must act in favor of increasing the predicted laboratory performance. This source is argued to be the interference effect from the wind-tunnel walls. This argument is backed up by observing the effect of reducing the lateral and vertical dimensions of the integration domain when performing field predictions, i.e. the effect of caving in the flow field. This analysis was done in [1] in order to estimate the minimum required dimensions of the integration domain to yield domain-dimension independent results, and is displayed in Fig. 6 reproduced from [1].

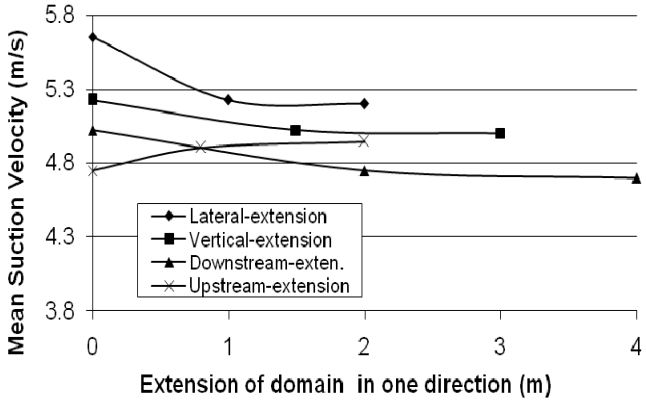


Figure 6. Effect of extending domain on predicted $V_{suc}$,[1].

Figure 6 shows clearly that the effect of expanding the integration domain in the lateral and vertical directions is to lower the predicted value of the mean suction velocity. Naturally, the opposite is also true, so that the effect of reducing the integration domain due to the need to comply to the location of the wind tunnel walls results in an over prediction of the suction velocity

## DISCUSSION OF FIELD & LABORATORY FLOWS

The effect of confinement of the wind tunnel walls is to decrease the lateral and vertical displacement of the approaching air streams as they reach the ventilator inlet; thus increasing the flow of air into the ventilator body. The latter causes an increase in flow velocity at throat section, thus decreasing the pressure there and consequently increasing the suction of air into the suction-pipe.

Moreover, since the wind tunnel is of the induced draft type, it is the total pressure at the inlet of the tunnel that equals atmospheric pressure, the static pressure being less by the balance of the dynamic head. Thus the static pressure of the approaching stream of air is less than in the case of the field flow. This reflects in a lower static pressure at the throat section than in the case of the field flow, and thus a larger pressure difference across the suction-inlet to drive the suction flow.

Both of the above mentioned effects work to increase the suction air flow. Figure 7 reveals the predicted flow under laboratory conditions over the diffuser section of the mid-plane of the ventilator. The vectors represent in both magnitude and direction the local velocity vectors.

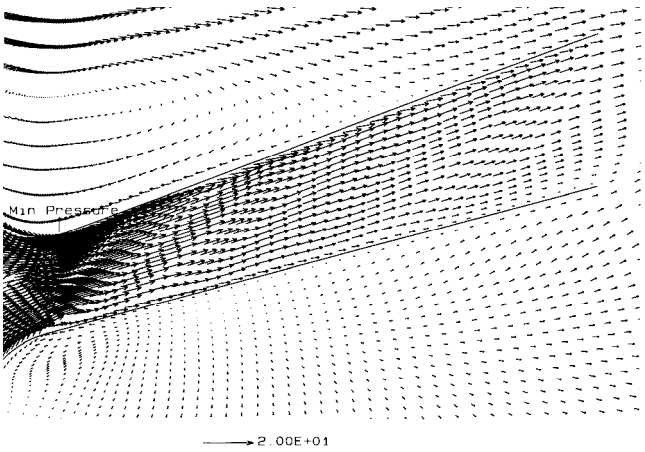


Figure 7. Velocity vectors under laboratory conditions,[2]

It is seen that the flow in the diffuser section is smooth, fairly uniform and forward flowing almost over the entire diffuser section.

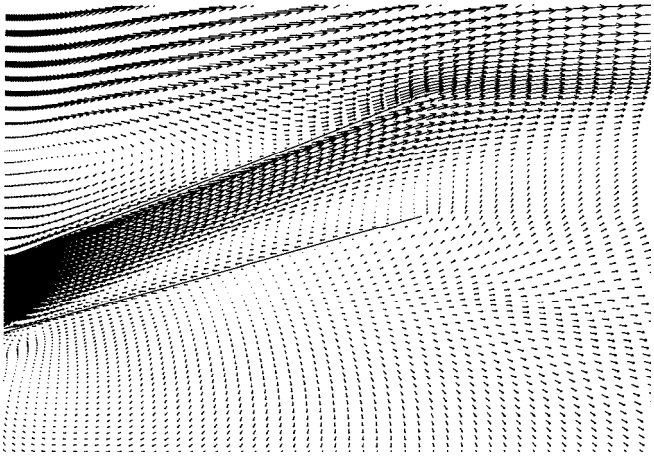

Figure 8. Velocity vectors under field conditions, [1].

Figure 8 reveals the corresponding velocity vectors under field conditions, again at the mid-plane of the ventilator. It is seen that the flow is nearly stagnant in the bottom half of diffuser and a weak recirculation zone appears close to bottom wall. Clearly the flow pattern at this plane is much less favorable than that revealed in Fig. 7 for laboratory conditions. Since the performance of the ventilator depends to a large extent on the degree of head recovery in the diffuser section, the more favorable flow will result in higher suction flow rates. All said however, it is only towards the middle plane of the ventilator that the flow is so unfavorable, and only so under field conditions.

Moreover, for both the field and laboratory conditions the flow is very smooth in the throat section upstream the diffuser,[1,2].

## SUMMARY & CONCLUSION

When the performance of the ventilator was measured experimentally under laboratory conditions it was found to be considerably better than what was predicted for field conditions employing a highly accurate, validated code. Further investigations showed that this was caused mainly by the difference between the approaching stream pressure boundary-conditions; a total pressure boundary condition more accurately representing the induced draft wind-tunnel entrance, whereas a static pressure condition better representing the atmospheric flow under field conditions. Other effects include interference from wind-tunnel walls and pressure losses in the measurement equipment (venturi-meter).

The work clearly demonstrates the importance of coupling experimental tests with corresponding predictions. It demonstrates how this should be conducted in order to assess the effect of deviation of laboratory conditions from actual operating conditions. In many applications, the performance characteristics in particular are derived solely from laboratory measurements, which by necessity must involve some degree of deviation from field conditions; this work shows that this may lead to misleading results.

## NOMENCLATURE

| | |
|---|---|
| $C_1$, $C_2$, $C_\mu$ | turbulence model constants |
| $C_\phi$ | convection term |
| $D_\phi$ | diffusion term |
| k | turbulence kinetic energy |
| $P_o$ | total pressure |
| p, $p_{st}$ | static pressure |
| $S_\phi$ | source term |
| $v_{suc}$ | suction velocity |
| *Greek letters* | |
| $\beta$ | turbulence model constants |
| $\varepsilon$ | rate of dissipation of k |
| $\mu_t$ | effective turbulence viscosity |
| $\eta_o$ | turbulence model constant |
| $\sigma_k$, $\sigma_\varepsilon$ | turbulence model constants |
| $\rho$ | mass density |

## REFERENCES

[1] M.A. Serag-Eldin, "Prediction of Performance of a Wind-Driven Ventilation Device," JWEIA, submitted for publication,2007.

[2] M.A. Serag-Eldin, "Experimental Validation of the Predicted Performance of a Wind Driven Venturi Ventilator", *Proc. of WCSET 2008, Paris, July 04-06, 2008, PWASET,* Vol. 30, pp.214-219.

[3] V. Yakhot and S. Orszag, "Renormalization Group Analysis of Turbulence. I.Basic Theory," *J. of Scientific Computing*, vol.I , No.1, pp.3-51.,1986.

 

[4] V. Yakhot and L.M. Smith, " The Renormalization Group, the ε-expansion and Derivation of Turbulence Models," *J. of Scientific Computing*, vol. 7, No.1., 1992.

[5] J.H. Ferziger and M. Peric, *Computational Methods for Fluid Dynamics*, 2nd edition. New York: Springer-Verlag, 1999.

[6] L.S. Carreto, A.D. Gosman, S.V. Patankar and D.B. Spalding, "Two Calculation Procedures for Steady Three-Dimensional Flow with Recirculation," *Proceedings of the 3rd Int. Conf. Num. Methods in Fluid Mechs*., vol II, pp.60-98, 1973,.

[7] J.F. Thompson, Z.U.Warsi and C.W. Mastin, "Boundary-fitted Coordinate Systems for Numerical Solution of Partial Differential Equations – A Review," *J. of Computational Physics*, vol.47, pp 1- 108, 1982.

[8] D.J. Anderson, *Computational Fluid Dynamics*, McGraw-Hill, London & New York, 1995.

[9] M.R. Malin, H.I.Rosten, D.B.Spalding and D.G.Tatchell, "Application of PHOENICS to Flow Around Ship's Hulls," *Proceedings of 2nd Int. Symposium on Ship Viscous Resistance*, Goteburg, Sweden, 1985.

[10] P.K. Hedberg, H.I.Rosten and D.B.Spalding, "The PHOENICS Equations", *CHAM Report TR/99*, CHAM U.K.

[11] B.E. Launder and D.B .Spalding, "The Numerical Computation of Turbulent Flows", *J. Computational Methods in Applied Mechanics and Eng.*, vol.3, pp. 269-289, 1974.

[12] E.O. Doebelin, *Measurement Systems: Application and Design*, McGraw-Hill: Tokyo, London and Sydney, p.472,Ch.7, 1976.